crystals

MDPI

Article

Application of the Improved Inclusion Core Model of the Indentation Process for the Determination of Mechanical Properties of Materials

Boris A. Galanov, Yuly V. Milman *, Svetlana I. Chugunova, Irina V. Goncharova and Igor V. Voskoboinik

Institute for Problems of Materials Science of NASU, 3 Krzhizhanovky Str., 03680 Kiev, Ukraine; gbaprofil@bk.ru (B.A.G.); yuly.milman@gmail.com (S.I.C.); irina@ipms.kiev.ua (I.V.G.); igor-d23@ipms.kiev.ua (I.V.V.)

* Correspondence: milman@ipms.kiev.ua; Tel.: +38-044-424-3184

Academic Editors: Ronald W. Armstrong, Stephen M. Walley, Wayne L. Elban and Helmut Cölfen
Received: 9 February 2017; Accepted: 14 March 2017; Published: 16 March 2017

Abstract: The improved Johnson inclusion core model of indentation by conical and pyramidal indenters in which indenter is elastically deformed and a specimen is elastoplastically deformed under von Mises yield condition, was used for determination of mechanical properties of materials with different types of interatomic bond and different crystalline structures. This model enables us to determine approximately the Tabor parameter $C = HM/Y_S$ (where HM is the Meyer hardness and Y_S is the yield stress of the specimen), size of the elastoplastic zone in the specimen, effective apex angle of the indenter under load, and effective angle of the indent after unloading. It was shown that the Tabor parameter and the size of elastoplastic deformation zone increase monotonically with the increase of the plasticity characteristic δ_H, which is determined in indentation experiments using the early elaborated by the several authors of this article method. The corresponding analytical dependencies were obtained and their physical nature is discussed. For the materials studied in this work, the Tabor parameter ranges from 1 to 4. At the same time, for structural metallic alloys its value is between 2.8 and 3.1 in agreement with the results obtained by Tabor. A very simple technique developed in this article allows one to determine from the standard indentation test not only the hardness of a material but also its yield stress and plasticity. This makes the indentation test results significantly more informative.

Keywords: mechanical properties; hardness; indentation; plasticity

1. Introduction

The study of mechanical properties of materials by the method of local loading with a rigid indenter is extensively used in practice. In indentation the Meyer hardness $HM = P/S$ (where P is the load on the indenter and S is the projection area of the hardness indent on the initial surface of the specimen) has a precise physical meaning of the average pressure under indenter and is usually determined.

Indentation models which describe theoretically the indentation process with the aim to determine other mechanical properties, particularly the yield stress of material Y_S, were proposed long ago and many times [1,2]. Among the developed models, the Johnson inclusion core model is the most successful [3,4].

The details of these investigations and historical information on this problem up to 1969 are presented in [3]. Thereafter, the concept of the inclusion core model was checked and investigated in many works (see, e.g., [5–9]). In [10], executed with the participation of several authors of this article, Johnson's model has been improved to describe the process of continuous indentation, in which not

only the sample, but also the indenter undergoes elastic-plastic deformation. In this improved model the elastic compression of the inclusion core under the indenter is taken into account for the first time, as well as the change in the apex angle of the indenter in the deformation process. In [10] for the description of such indentation process the system of five equations was derived, which has been used to study the deformation of diamond during indentation by the diamond indenter. In this paper, the model [10] is simplified for the case where only the sample is deformed elastically-plastically, and the indenter is deformed elastically. The advantages of the model [10] are preserved in this paper by taking into account the compression of the core under indenter and the change of the indenter shape as a result of elastic deformation. Simplification of the model [10] reduced the number of equations from five to three (see the system of Equations (26) in [10] and the system (1) in this article). The system (1) is used in this study to analyze the deformation process during indentation of materials with different types of interatomic bonds and various crystalline structures, to establish the functional relationship between the Tabor parameter C [11] and the plasticity of the material ($C = HM/Ys$, where HM is the Meyer hardness and Ys is the yield stress of the specimen), as well as for development of the simple method for determination of the yield stress as a result of standard determination of hardness.

2. Theoretical Background. Scheme and Equations of the Improved Model

Figure 1 shows a scheme in a spherical coordinate system $0r\theta\varphi$ of a model of contact interaction of a conical indenter and specimen, in which a hydrostatic core of radius c forms. The non-deformed indenter is shown by a dashed line, and the following notations are used: ψ is the angle between the surface of the indenter and the indenter axis x_i under load; $0 \le r \le c$ is the region of the core; $c \le r \le b_S$ is the spherical layer of the specimen where elastoplastic deformations occurred; $r \ge b_S$ is the region of elastic deformation of the specimen. Strains are assumed to be sufficiently small.

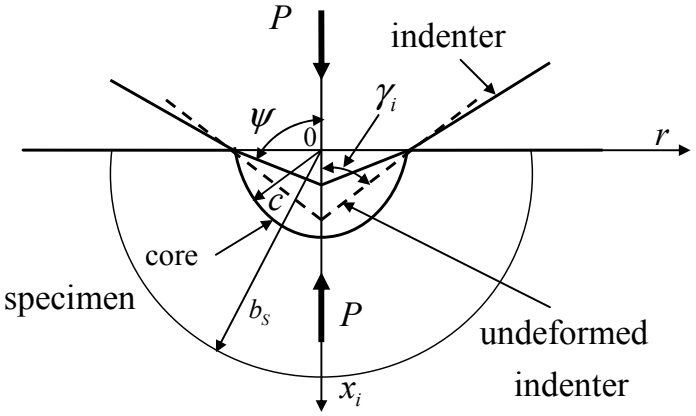

Figure 1. Scheme of interaction of an indenter and a specimen under a load P in a spherical coordinate system $0r\theta\varphi$, $HM = P/(\pi c^2)$.

Dislocation approach to the mechanism of deformation during indentation is being developed intensively ([12–18], etc.). In the framework of the dislocation theory, the zone of elastoplastic deformation with the radius b_S is the zone with a sharp increase in the dislocation density around the indentation imprint with a symmetry center at the very point 0 in Figure 1. Dislocations are nucleated near the indenter and move in the radial directions to the boundaries of the elastoplastic zone under the action of shear stress, caused by the load on indenter [19]. The comparison of calculated values of b_S with the experimental data is given in the Section 3.6.

During continuous penetration of the elastic indenter, the core increases at the expense of the elastoplastic zone of the specimen. This proceeds on its boundary, where the material of this zone is compressed by the pressure of the core, which exceeds the pressure in the elastoplastic zone (in passing the boundary of the core, the jump of pressure and volume strain is observed; shear stresses, which are absent in the hydrostatic core, also change abruptly). During such penetration, the

material of the elastoplastic zone is additionally densified on the boundary of the core by a pressure $\Delta p_S = 2Y_S/3$ (caused by the jump of pressure Δp_S on this boundary) and joined to the material of the core.

As mentioned above, this model has three transcendental equations for three unknown quantities: yield stress Y_S, the relative size of the elastoplastic zone $x = b_S/c$ and $z = \cot\psi$:

$$\begin{cases} z = \cot\psi = \cot\gamma_i - 2HM/E_i^*, & (1a) \\ (1-\theta_S Y_S)\cdot(x^3 - \alpha_S) = z\beta_S/Y_S, & (1b) \\ (2/3 + 2\ln x) - HM/Y_S = 0, & (1c) \end{cases}$$

where the notation $\alpha_S = \frac{2(1-2\nu_S)}{3(1-\nu_S)}$, $\beta_S = \frac{E_S}{6(1-\nu_S)}$, $\theta_S = \frac{2(1-2\nu_S)}{E_S}$ and $E_i^* = \frac{E_i}{1-\nu_i^2}$ is used, E is the Young's modulus, ν is the Poisson's ratio, γ is the angle between the surface and the axis x_i of the conical non-deformed indenter. Subscripts i and s correspond to the indenter and specimen, respectively. The solution of this system for unknowns (z, x, Y_S) determines approximately the stress-strain state of the specimen in accord with the proposed model. As it is seen from Equation (1c) the Tabor constant

$$C = HM/Y_S = 2/3 + 2\ln x, \quad (2)$$

The system of Equations (1) takes into account the elastic compressibility during formation of the core, and, thus, the proposed model develops the model considered in [3,4]. Equation (1a) corresponds to Equation (17) of the work [10] at $\gamma_{iR} = \gamma_i$, Equation (1b) corresponds to the first equation of the system (26) of the work [10], and Equation (1c) corresponds to the fourth equation of the system (26) of the work [10].

The influence of compressibility during formation of the core, as it follows from [10] is determined by the value of $\theta_S Y_S$. This value increases with increase in the ratio Y_S/E_S and with decrease in the Poisson's ratio ν. The evaluation of $\theta_S Y_S$ shows that the ratio Y_S/E_S can attain 0.1 for covalent crystals, and $\theta_S Y_S$ becomes substantial as compared to 1. For the same crystals, ν has a minimum value, which is particularly small for diamond ($\nu = 0.07$). Diamond was not investigated in the present work because its deformation is purely elastic at room temperature. Features of the diamond deformation during indentation by diamond indenter are considered in [10]. However, we can evaluate the quantity Y_S/E_S on the basis of the Meyer hardness of diamond at room temperature HM = 150 GPa [20] assuming that, as for high-hardness ceramics, for diamond, $Y_S \approx HM$. For diamond and for the value E = 1200 GPa, we obtain $\theta_S Y_S \approx 0.23$, i.e., the compressibility of the deformation core is particularly substantial for diamond and high-hardness ceramic materials. For metals, at $Y_S/E_S \approx 0.002$, and if $\nu = 0.35$, the value of $\theta_S Y_S = 0.001$, is much smaller than 1, and taking into account the compressibility of the material during formation of the core hardly influences on the obtained results.

For the residual conical indent in the specimen, the effective angle γ_{SR} after its elastic unloading has the value ([10], Equation (16))

$$\cot\gamma_{SR} = \cot\psi - 2HM(1-\nu_S^2)/E_S, \quad (3)$$

where the term $2HM(1-\nu_S^2)/E_S$ takes account of the elastic recovery of angle ψ and elastic deflection component of the specimen surface.

The considered model was elaborated for the case of penetration of a cone with an apex angle 2γ. The following relations between the apex angles of equivalent conical and pyramidal (trihedral and tetrahedral) indenters were proposed in [10],

$$\cot\gamma_i = \sqrt{\pi}\cot\gamma_V/2 = \sqrt[4]{\pi^2/27}\cot\gamma_B, \quad (4)$$

where γ, γ_V, γ_B are the apex angles of conical, tetrahedral (e.g., Vickers indenters, γ_V = 68°), and trihedral (e.g., Berkovich indenters, γ_B = 65°) indenters, respectively.

3. Results and Discussion

3.1. Comparative Analysis of the Deformation Process during Indentation of Materials with Different Types of Interatomic Bond and Different Crystalline Structures

In this work, results of measurement of the Vickers microhardness obtained by the authors, a substantial part of which was published [18,21–25], were used. For most presented results, the load on the indenter was close to 2 N. For the analysis of features of deformation in indentation, we chose unalloyed polycrystalline and single-crystalline metals with FCC, BCC, and HCP lattices; a number of intermetallics (Al_3Ti, $Al_{61}Cr_{12}Ti_{27}$, and $Al_{66}Mn_{11}Ti_{23}$); single-crystals of refractory carbides (WC, NbC, TiC, ZrC, and SiC), covalent crystals of Si and Ge, and partially covalent Al_2O_3 and LaB_6; amorphous alloys ($Fe_{83}B_{17}$, $Fe_{40}Ni_{38}Mo_4B_{18}$, and $Co_{50}Ni_{10}Fe_5Si_{12}B_{17}$) and quasicrystals ($Al_{63}Cu_{25}Fe_{12}$ and $Al_{70}Pd_{20}Mn_{10}$). An investigation was also performed for steel with 0.45% C and 5083 aluminum alloy.

The characteristics of the studied materials are presented in Table 1. The microhardness *HM* was calculated from the value of *HV* (*HM* = 1.08 *HV*). In calculations for the diamond indenter, E_i = 1200 GPa and ν_i = 0.07 were taken.

The analysis of the deformation process in microindentation was performed on the basis of the developed inclusion core model of indentation with the use of the system of Equations (1). The parameter *z* was calculated from Equation (1a), and then the system of Equations (1b) and (1c) was solved to determine the yield strength Y_S and the relative size of the elastoplastic zone in the specimen $x = b_S/c$.

The apex angle of the equivalent conical indenter under load ψ was calculated by the relation $z = cot\ \psi$. The apex angle of the conical hardness indent in the specimen after unloading of the indenter γ_{SR} was calculated by Equation (3).

In accordance with [10,21], the mean plastic strain on the contact area of the indenter and specimen ε_p in the direction of the force *P* applied to the indenter was calculated by Equation (5), the elastic strain ε_e, corresponding to the elastic deflection component of the specimen surface, was computed by (6), and the total strain ε_t was calculated by (7)

$$\varepsilon_p = \ln\sin\gamma_{SR} = -\ln\sqrt{1+\cot^2\gamma_{SR}} < 0, \quad (5)$$

$$\varepsilon_e = -(1+\nu_S)(1-2\nu_S)HM/E_S, \quad (6)$$

$$\varepsilon_t = \varepsilon_e + \varepsilon_p. \quad (7)$$

The plasticity characteristic δ_H (introduced in [18]) was evaluated by formula (8) in section 3.2.1. The obtained results are presented in Table 1, in which groups of materials are located in the order of decreasing plasticity characteristic δ_H. It is seen, that the Tabor parameter *C* decreases simultaneously with a decrease δ_H within each group of materials of Table 1, and at the comparison of values C and δ_H of the different groups.

For the most plastic materials with a FCC lattice, *C* = 3.8–4. For metals with BCC and HCP structures, $C \approx 3$, which corresponds to the Tabor concept [11].

Among the other studied materials, intermetallic compounds have values of $C \approx 2$, that are close to those for metals.

Among the studied refractory compounds, the lowest value of *C*, even smaller than 1, is observed for SiC and Al_2O_3. These crystals also have the smallest plasticity.

Among refractory compounds, carbide WC, as is known [24,25], is distinguished by increased plasticity δ_H = 0.81, and, for it, *C* = 1.89, that is higher than for other refractory compounds. For covalent crystals Si and Ge, $C \approx 1$. At the same time Ge has a somewhat higher plasticity and higher value of *C*. However, it should be taken into account that, in these crystals, indentation leads to the

semiconductor–metal phase transition [26,27], which complicates the discussion of results obtained for them.

Table 1. Mechanical characteristics of materials (Meyer hardness *HM*, Young modulus E_S, and Poisson's ratio ν_S) and characteristics calculated according to the core indentation model (Tabor parameter *C*, yield stress Y_S, plasticity characteristic δ_H, relative size of elastoplastic zone *x*, apex angle of indenter under load ψ, and relaxed effective apex angle of a hardness indent γ_{SR}).

Materials		*HM*, GPa	E_S, GPa	ν_S	$C = HM/Y_S$	Y_S, GPa	δ_H	$x = b_S/c$	ψ, deg.	γ_{SR}, deg.
FCC metals	Al	0.173	71	0.35	4.02	0.043	0.99	5.33	68.01	68.12
	Au	0.270	78	0.42	3.86	0.07	0.99	4.84	68.02	68.27
	Cu	0.486	130	0.343	3.74	0.13	0.98	4.47	68.04	68.32
	Ni	0.648	210	0.29	3.81	0.17	0.98	4.68	68.05	68.29
BCC metals	Cr	1.404	298	0.31	3.42	0.41	0.97	3.98	68.10	68.47
	Ta	0.972	185	0.342	3.35	0.29	0.97	3.88	68.07	68.48
	V	0.864	127	0.365	3.20	0.27	0.97	3.54	68.06	68.58
	Mo (111)	1.998	324	0.293	3.17	0.63	0.96	3.52	68.14	68.64
	Nb	0.972	104	0.397	2.94	0.33	0.96	3.16	68.07	68.76
	Fe	1.512	211	0.28	3.02	0.50	0.95	3.29	68.11	68.69
	W (001)	4.320	420	0.28	2.73	1.58	0.92	2.80	68.31	69.15
HCP metals	Ti	1.112	120	0.36	2.93	0.38	0.95	3.09	68.08	68.79
	Zr	1.156	98	0.38	2.75	0.42	0.95	2.83	68.08	68.97
	Re	3.024	466	0.26	3.09	0.63	0.95	3.38	68.22	68.75
	Mg	0.324	44.7	0.291	2.94	0.11	0.95	3.3	68.02	68.60
	Be	1.620	318	0.024	3.05	0.53	0.94	3.35	68.12	68.56
	Co	1.836	211	0.32	2.91	0.63	0.94	3.10	68.13	68.82
Intermetallics (IM)	$Al_{66}Mn_{11}Ti_{23}$ (IM_3)	2.203	168	0.19	2.42	0.91	0.87	2.42	68.16	69.27
	$Al_{61}Cr_{12}Ti_{27}$ (IM_2)	3.456	178	0.19	2.08	1.66	0.81	2.03	68.25	69.90
	Al_3Ti (IM_1)	5.335	156	0.30	1.67	3.19	0.76	1.65	68.38	71.16
Metallic glasses (MG)	$Fe_{40}Ni_{38}Mo_4B_{18}$ (MG_2)	7.992	152	0.30	1.25	6.39	0.62	1.34	68.58	72.90
	$Co_{50}Ni_{10}Fe_5Si_{12}B_{17}$ (MG_3)	9.288	167	0.30	1.19	7.80	0.60	1.30	68.67	73.25
	$Fe_{83}B_{17}$ (MG_1)	10.044	171	0.30	1.14	8.84	0.58	1.26	68.73	73.58
Quasicrystalls (QC)	$Al_{70}Pd_{20}Mn_{10}$ (QC_2)	7.560	200	0.28	1.55	4.88	0.71	1.55	68.54	71.67
	$Al_{63}Cu_{25}Fe_{12}$ (QC_1)	8.024	113	0.28	0.97	8.30	0.48	1.16	68.58	74.54
Refractory compounds	WC (0001)	18.036	700	0.31	1.89	9.56	0.81	1.84	69.31	71.40
	NbC (100)	25.920	550	0.21	1.22	21.26	0.54	1.32	69.89	74.02
	LaB_6 (001)	23.220	439	0.20	1.13	20.51	0.50	1.26	69.69	74.34
	TiC (100)	25.920	465	0.191	1.08	24.07	0.46	1.23	69.89	74.83
	ZrC (100)	23.760	410	0.196	1.06	22.48	0.46	1.22	69.73	74.85
	Al_2O_3 (0001)	22.032	323	0.23	0.94	23.40	0.41	1.15	69.60	75.56
	α-SiC (0001)	32.400	457	0.22	0.87	37.24	0.36	1.11	70.38	76.77
Covalent crystals	Ge (111)	7.776	130	0.21	1.10	7.06	0.49	1.24	68.56	73.75
	Si (111)	11.340	160	0.22	0.96	11.84	0.42	1.16	68.82	74.99
Industrial alloys	Steel 0.45%C	1.890	204	0.285	2.74	0.69	0.93	2.79	68.14	68.88
	Al alloy #5083	1.030	70.1	0.33	2.51	0.41	0.91	2.49	68.07	69.23

In view of the established correlation of the Tabor parameter *C* with the plasticity characteristic δ_H, it seems reasonable to consider the relation of these characteristics more thoroughly to elucidate the physical nature of the Tabor parameter *C*. The relation between *C* and δ_H seems to be particularly interesting because both these characteristics relate the hardness to the mechanical properties of the material, namely, to the yield strength (Tabor parameter *C*) and to the plasticity of the material (plasticity characteristic δ_H).

3.2. Relation between the Tabor Parameter $C = HM/Y_S$ and Plasticity Characteristic δ_H

3.2.1. Plasticity Characteristic δ_H Determined by Indentation

In modern physics plasticity is determined by the tendency of a material to undergo residual deformation under load [28,29].

The frequently used plasticity characteristics (elongation of a specimen to fracture δ and its reduction of the area to fracture Ψ) do not correspond to the physical definition of plasticity and must be considered only as convenient technological tests [18,21,30], which can be used for only metals having some elongation to fracture. For a large number of modern materials, the value $\delta = 0$

and cannot characterize their mechanical behavior. The plasticity characteristic satisfying the physical definition of plasticity was proposed in [18] in the form of the dimensionless parameter

$$\delta^* = \varepsilon_p / \varepsilon_t = 1 - \varepsilon_e / \varepsilon_t, \quad (8)$$

where ε_p, ε_e, and ε_t are, respectively, the plastic, elastic, and total strain, and $\varepsilon_t = \varepsilon_p + \varepsilon_e$.

The considered plasticity characteristic δ^* can be determined in any methods of mechanical tests (tension, compression, and bending) and, as shown in [18,21], in indentation.

It is seen from expression (8) that δ^* depends on the total strain ε_t, which follows directly from the definition of plasticity δ^* presented above.

Since the plasticity δ^* depends on the strain ε_t, a comparison of the plasticity of different materials should be performed at a representative strain $\varepsilon_t \approx const$. In tensile test, in the first stages of loading, $\varepsilon_t = \varepsilon_e$, and plastic strain is absent, i.e., the material does not retain a part of strain after unloading. For this reason representative strain ε_t must be sufficiently large (7%–10%). It is natural that, in the case of standard tensile and compression test methods, this characteristic can be determined only for sufficiently plastic metals. At the same time, the condition $\varepsilon_t \approx const$ is automatically fulfilled in indentation of materials using a pyramidal indenter, e.g., a tetrahedral Vickers pyramid or trihedral Berkovich pyramid, and the degree of total strain under these indenters lies in the interval indicated above ($\varepsilon_t \approx 7.6\%$ for a tetrahedral Vickers indenter, and $\varepsilon_t \approx$ 9.8% for a trihedral Berkovich indenter).

During indentation, the small volume of the deformed material and a specific character of strain fields decrease the susceptibility to macroscopic fracture. This enables one to determine the hardness and plasticity characteristic for most materials even at cryogenic temperatures.

In [18,21] it was shown that, for a pyramidal indenter, the plasticity characteristic can be determined in indentation in the form

$$\delta_H = 1 - \frac{HM}{E_S \cdot \varepsilon_t}\left(1 - \nu_S - 2\nu_S^2\right). \quad (9)$$

In particular, for a Vickers indenter, taking into account that $HV = HM \sin\gamma$, $\gamma = 68°$, and $\varepsilon_t = 7.6\%$, we have

$$\delta_H = 1 - 14{,}3 \cdot \left(1 - \nu_S - 2\nu_S^2\right) HV / E_S, \quad (10)$$

The introduction of the plasticity characteristic δ_H made it possible to classify practically all (plastic and brittle materials in standard mechanical tests) on the basis of their plasticity [18,21,22]. A dependence of δ_H on the temperature, strain rate, and structural factors has been established [18,21,30]. It was possible to introduce the notion of theoretical plasticity for perfect crystals in which theoretical strength is attained [30]. It was experimentally shown that there exists a critical value of the plasticity characteristic $\delta_{H\,cr} \cong 0.9$. At smaller values of δ_H, the plasticity in tensile tests is $\delta = 0$ or has a very low value. The plasticity characteristic δ_H is fairly extensively used in works of different authors (e.g., [31–33]).

The values of the plasticity characteristic δ_H for the materials studied in the present work are presented in Table 1, which enables us to compare them with the Tabor parameter C.

Consider the theoretical relation between C and δ_H. It follows from Equation (2) that the parameter C is completely determined by the relative size of the elastoplastic zone $x = b_S/c$. This is why we first calculate the relation between x and the plasticity characteristic δ_H.

3.2.2. Relation between the Relative Size of the Elastoplastic Zone $x = b_S/c$ and the Plasticity Characteristic δ_H

As noted in Section 2, for metals, the quantity $\theta_S Y_S$ can be neglected as compared to 1 in Equation (1b). Substituting Y_S from (1c) into (1b), we find the following equation for the determination of x for metals:

$$x^3 - \alpha_S = \frac{E_S z\left(\frac{2}{3} + 2\ln x\right)}{6(1-\nu_S)HM}, \tag{11}$$

where $\alpha_S = \frac{2(1-2\nu_S)}{3(1-\nu_S)}$.

Determining HM/E_S from (10) and substituting its value into (11), for the Vickers indenter we get the following explicit dependence of δ_H on the relative size of the elastoplastic deformation zone x:

$$\delta_H = 1 - \frac{2{,}21z\left(\frac{2}{3} + 2\ln x\right)}{x^3 - \alpha_S}\lambda_S, \tag{12}$$

where $\lambda_S = \frac{1-\nu_S-2\nu_S^2}{1-\nu_S} = 1 - 2\frac{\nu_S^2}{1-\nu_S}$.

It follows from Equation (12) and Figure 2 that δ_H is predominantly determined by the quantity x, but the parameters z and λ_S exert some influence on the relation between δ_H and x. For metals, the parameter z is practically equal to $z \approx cot\ \gamma$ because the angle ψ for them differs very slightly from an angle γ = 68° (see Table 1). Therefore, it can be assumed that $z \approx const$. However, the parameter λ_S varies somewhat for metals having different values of Poisson's ratio ν_S, which leads to an insignificant scatter of experimental results relative to the averaged curve in Figure 2.

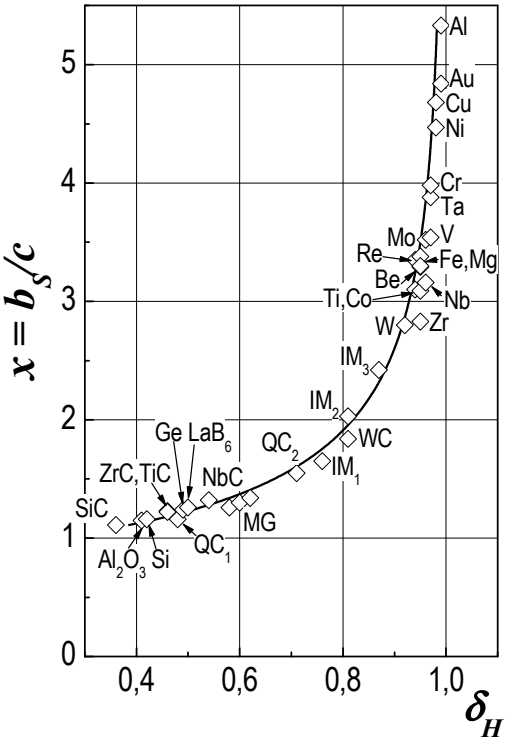

Figure 2. Relation between the plasticity characteristic δ_H and the relative size of the elastoplastic deformation zone x. Curve was constructed on the basis of Equation (12) for z = 0.38 and ν_S = 0.27.

For metals the results of calculation of δ_H by (10) and (12) practically coincide.

Formula (12) was used for the calculation of the dependence $x(\delta_H)$ shown in Figure 2. In this case, the values of the parameters z and ν_S were varied. The smallest mean square error equal to 0.06% was obtained for z = 0.38 and ν_S = 0.27. Thus, it was shown that Equation (12) with the values of the parameters z = 0.38 and ν_S = 0.27 can be used with an accuracy sufficient for practice not only for metals, but also for other materials studied in the work.

The experimental data and theoretical curve shown in Figure 2 indicate that the relative size of the elastoplastic deformation zone during indentation $x = b_S/c$ is mainly determined by the plasticity characteristic δ_H. The value of x increases monotonically with increasing δ_H. In this case, x changes from values close to 1 for ceramic materials to $x = 5.33$ for aluminum.

3.2.3. Yield Strength Y_S and Tabor Parameter HM/Y_S in the Considered Model

Figure 3 shows the relation between the Tabor parameter $C = HM/Y_S$ and plasticity characteristic δ_H. It is seen that the experimental dots for all studied materials lie on practically one curve.

To calculate the theoretical dependence $C(\delta_H)$ for the studied materials shown in Figure 3, formulas (1c) and (12) were used. We obtained the next Equation:

$$\delta_H = 1 - \frac{2{,}21zC\lambda_S}{\exp(1{,}5C - 1) - \alpha_S}, \quad (13)$$

It is seen from Figure3 that this equation satisfactorily describes the experimental results.

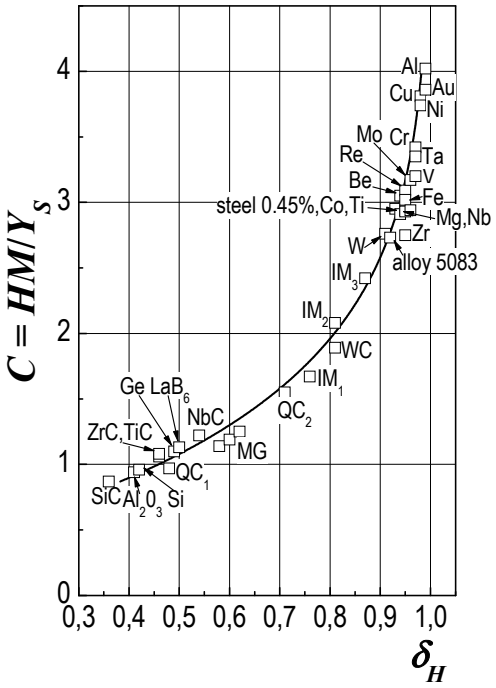

Figure 3. Relation between the Tabor parameter $C = HM/Y_S$ and the plasticity characteristic δ_H. Curve was constructed on the basis of Equation (13) for $z = 0.38$ and $\nu_S = 0.27$.

It should also be noted that, by analogy with $\delta_{H\,cr}$, the notion of the critical value of the Tabor parameter $C_{cr} = HM/Y_S \approx 2.6$ can be introduced. As is seen in Figure 3, this value corresponds to $\delta_{H\,cr} = 0.9$. Therefore, only for $C > 2.6$, the materials have a substantial macroscopic plasticity in tensile tests.

3.3. Physical Nature of Increase of the Tabor Parameter $C = HM/Y_S$ with Increase in the Plasticity δ_H

During indentation of low-plasticity materials, the elastoplastic deformation zone is small and its radius b_S exceeds slightly the radius of the penetrated indent c. In this case, $C \approx 1$ and $HM \approx Y_S$. However, as shown in the present work, with increase in the plasticity δ_H, the size of the elastoplastic deformation zone increases substantially, and, in most plastic materials, the value of b_S/c increases to more than 5. Therefore, during penetration of an indenter into plastic materials, deformation occurs not only under the indenter, but also in a hemisphere with a radius b_S, exceeding substantially the radius of the hardness indent c. In order for the plastic deformation to occur on a large hemisphere, the pressure $p = HM$ on the contact area of the indenter and specimen must exceed substantially the

yield strength Y_S. The higher ductility of the material, the greater the size of elastic-plastic deformation zone and, hence, the pressure p and the Tabor parameter C should be higher. The mathematical relation between $C = HM/Y_S$ and the plasticity characteristic δ_H is described by Equation (13) and is shown in Figure 3.

3.4. Relaxed Effective Apex Angle of a Hardness Indent γ_{SR} and Apex Angle of an Indenter under Load ψ

It is seen from Table 1 and Figure 4 that the relaxed apex angle of the hardness indent γ_{SR} can be much larger than the corresponding angle of the indenter $\gamma = 68°$. As is seen in Figure 4, the value of γ_{SR} correlates with the plasticity characteristic δ_H and can be described by the linear equation $\gamma_{SR} = 80.64 - 12.55\ \delta_H$. The correlation between γ_{SR} and δ_H shows once again the fundamental character of the plasticity characteristics δ_H.

It is obvious from Table 1 that, for metals, the value of the apex angle of indenter under load ψ differs very slightly from the value of γ. However, for high-hardness materials ψ can exceed 70°.

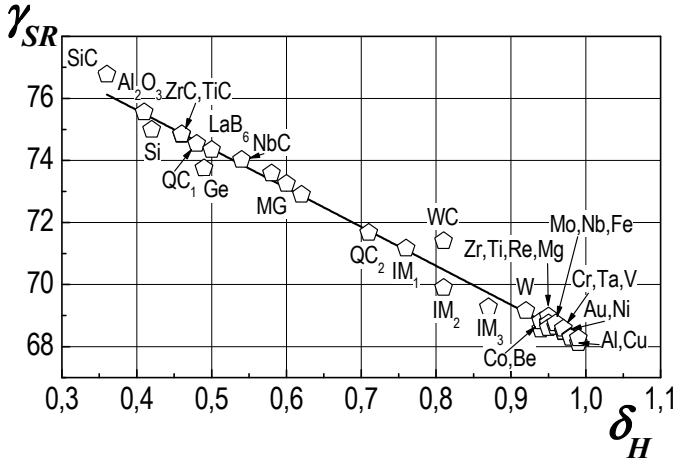

Figure 4. Dependence of the relaxed apex angle of a hardness indent γ_{SR} on the plasticity characteristic δ_H.

3.5. Simple Method of Determination of the Tabor Parameter $C = HM/Y_S$ and Yield Strength Y_S from the Hardness HM Determined with a Pyramidal Indenter

The results presented above enable us to propose a very simple method of determination of the Tabor parameter C and yield strength Y_S from the hardness HM determined with a Vickers indenter. In this method, the plasticity characteristic δ_H is calculated by the simple formula (12), the Tabor parameter C is determined from the curve shown in Figure 3 or calculated by Equation (13), and the yield strength is calculated by the formula $Y_S = HM/C$. The simplicity of the described technique makes it possible to use it extensively in indentation by the Vickers method. The authors think that the determination of the plasticity characteristic δ_H and yield strength Y_S raises significantly the informativeness and efficiency of the indentation technique. It should be noted that the simplified calculation of the Tabor parameter C and yield strength Y_S can also be carried out in the case of measuring the hardness HM by a trihedral Berkovich indenter. In this case, for the determination of the plasticity characteristic δ_H, it is necessary to use relation (9) at $\varepsilon_i \approx 9.8\%$.

3.6. Experimental Check of the Values of the Tabor Parameter $C = HM/Y_S$ and the Radius of Elastoplastic Zone b_S.

As is seen from Figure 3 and Table 1, the value of the Tabor parameter C changes quite strongly for different materials. Why did the parameter C range from 2.8 to 3.1 in the Tabor tests? This can be explained by the fact that Tabor tested structural metallic alloys. These alloys are usually hardened by alloying and heat treatment, but hardening is limited by the necessity to have good plasticity, which is measured as elongation to fracture δ, and usually $\delta \approx 10\%–20\%$ for these alloys. According

to the data of the authors of the present paper, such values of δ corresponds to the plasticity characteristic δ_H = 0.93 − 0.95. According to Figure 3, at this value of δ_H, the Tabor parameter *C* is actually equal to 2.8–3.1 for different materials.

In a number of earlier performed works (e.g., [3–6]), it was shown that for ceramic materials the Tabor parameter *C* approaches 1 as in the present work.

It follows from Figure 3 and Table 1 that materials with a plasticity characteristic lower than that for metals (δ_H < 0.9: intermetallics, refractory compounds, quasicrystals, metallic glasses etc.) must also be characterized by a lower value of $C = HM/Y_S$. An experimental check of the values of *C* for these materials is complicated (or practically impossible) because of their insufficiently high plasticity in compression tests for the determination of Y_S at a total strain $\varepsilon_t \approx 7.6\%$. However, the values of *C* for these materials obtained in the present paper are fairly predictable because the values of the plasticity characteristic δ_H and the relative size of the elastoplastic deformation zone b_S/c for them are intermediate between those for metals and ceramics.

It seemed reasonable to check the high value $C \approx 4$ for pure aluminum, as a representative of the most plastic metals with a FCC lattice.

For this purpose, we prepared specimens of aluminum of 99.98% purity for uniaxial compression tests. The specimens had a diameter d = 5 mm and a height h = 6 mm. They were prepared from a commercial ingot and annealed in vacuum at a temperature of 400 °C for 1 h. The mean grain size was equal to 93 μm. The yield stress $\sigma = Y_S$ in compression to $\varepsilon_t \approx 7.6\%$ was equal to 41 MPa. As is seen from Table 1, the hardness is HM = 173 MPa. Therefore, $C_{exp} = HM/\sigma_{7.6\%} = 4.2$, which confirms the high value of the parameter *C* for aluminum, which even somewhat exceeds the value calculated using the developed model $C \approx 4.02$. In this case, for the studied aluminum, δ_H = 0.99, which, according to Figure 3 and Equation (13), corresponds to $C \approx 4$–4.2.

The experimental check of the values of the Tabor parameter *C* by the uniaxial compression test method was also performed for 5083 aluminum alloy and carbon steel containing 0.45% C. These materials were tested in the as-delivered state. The obtained results are presented in Table 2. It is seen that the values of the yield strength Y_S and Tabor parameter *C* obtained by the indentation method (with calculation by Equations (1) and (2)) agree well with those obtained in mechanical tests. The values of *C* and δ_H for these materials are also shown in Figure 3 and coincide satisfactorily with the calculated curve $C = f(\delta_H)$.

Table 2. Results of compression mechanical tests (yield stress at tension (ε_t = 7.6%) $Y_{7.6\%}$, the value of C_{exp} in tension test).

Material	$Y_{7.6\%}$, GPa	C_{exp}
Al	0.041	4.21
Al alloy #5083	0.373	2.76
Steel 0.45%C	0.64	2.95

For comparison of the actual size of the elastoplastic deformation zone with the calculated value of b_S, results of the work [34], in which dislocation rosettes around indentation were investigated for Mo (001) single crystal by etch pits method, were used. Additionally, in the present work, dislocation rosettes around indentation made at 300 °C were investigated. In Figure 5 the circles with radius b_S are plotted on dislocation rosettes around the indentations. At the room temperature (Figure 5a) the anisotropy of the dislocation velocity in different crystallographic directions is observed, but at 300 °C such anisotropy is absent (Figure 5b). It is seen, that in both cases, the calculated values of b_S are in satisfactory agreement with the average values of the areas in which plastic deformation has occurred and dislocation density has increased.

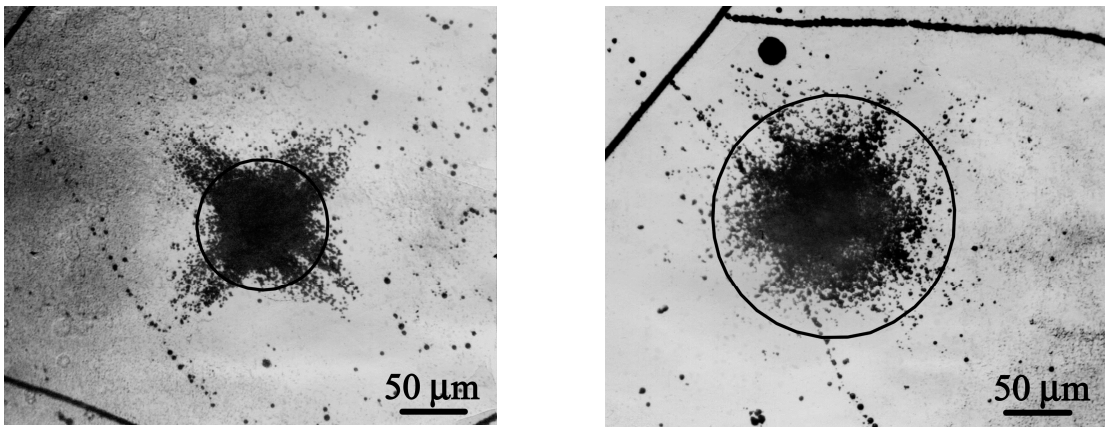

(**a**) (**b**)

Figure 5. Dislocations around indentation print for single crystal Mo (001), revealed by etch pits method. The circles with radius b_S are plotted on dislocation rosettes: (**a**) t = 20 °C, HM = 1.998 GPa, b_S = 47.7 μm [34]; (**b**) t = 300 °C, HM = 1.026 GPa, b_S = 87.2 μm, present work.

4. Conclusions

1. The developed inclusion core model of indentation by conical and pyramidal indenters makes it possible to carry out an analysis of the mechanical behavior of materials in indentation with the determination of the Tabor parameter $C = HM/Y_S$, yield strength Y_S, relative size of the elastoplastic deformation zone under an indenter b_S/c (see Figure 1), effective angle of a relaxed hardness indent γ_{SR}, and effective angle of an indenter under load ψ. In this case, for the first time, the elastic compressibility of the deformation core is taken into account. An analysis of the mechanical behavior in the indentation of materials with different types of interatomic bond and different crystalline structures has been carried out using the developed model.

2. It has been shown that the main quantities of the developed indentation model (the Tabor relation $C = HM/Y_S$ and relative size of the elastoplastic deformation zone b_S/c) correlate precisely with the determined in indentation plasticity characteristic δ_H = ***plastic strain/total strain***, which was introduced in [18]. The Tabor parameter C and the size of the elastoplastic deformation zone b_S/c increase monotonically with increasing plasticity characteristics δ_H. The Tabor parameter ranges from 1 for ceramic materials to 3.8–4.0 for the most plastic FCC metals. In structural metallic alloys, combining a high strength with an elongation at fracture δ = 10%–20% (which corresponds to δ_H = 0.93–0.95), C = 2.8–3.1, which agrees with the results obtained by Tabor. The relative size of the elastoplastic deformation zone b_S/c changes from 1 for ceramic materials to 5.3 for aluminum. The calculated size of b_S is in the satisfactory agreement with the average values of the area in which plastic deformation under indenter is occurred and dislocation density is increased.

3. On the basis of the developed inclusion core model of indentation, analytical expressions relating C and b_S/c to the plasticity characteristic δ_H have been obtained. These expressions agree sufficiently well with the obtained experimental results and make it possible to calculate C and b_S/c from the value of the plasticity characteristic δ_H. To determine more exactly all parameters, it is necessary to solve the system (1) of three equations with three unknowns.

4. The physical nature of increase of the Tabor parameter $C = HM/Y_S$ with increasing plasticity is explained by the fact that with increase in the plasticity, the elastoplastic deformation zone b_S/c increases and b_S can substantially exceed the radius of the hardness indent c. This is why the pressure $p = HM$ on an area of radius c must provide plastic deformation not only under the indenter, but also in a hemisphere of radius b_S. Naturally, in this case, the pressure p must be substantially higher than the yield strength Y_S.

5. It has been shown that it is reasonable to introduce the notion of the critical value of the Tabor parameter C_{cr} = 2.6. Only at C > 2.6, materials have substantial macroscopic plasticity in tensile tests.

6. A very simple technique of determination of the Tabor parameter $C = HM/Y_S$ and yield strength Y_S from results of standard indentation has been proposed. In this technique, the plasticity

characteristic δ_H is determined by the simple formula (10), and the Tabor parameter is determined from the calibration plot $C = f(\delta_H)$ shown in Figure 3. The yield strength Y_S is calculated by the formula $Y_S = HM/C$.

7. Thus, the inclusion core model of indentation developed in the present work and the earlier proposed technique of determination of the plasticity δ_H enable us to calculate both the yield strength and plasticity characteristic from the value of the hardness HM and elastic characteristics of the material. The authors think that the determination of the plasticity characteristic δ_H and yield strength Y_S make the indentation technique substantially more informative and efficient.

Acknowledgments: This work supported by the Program "Development of the theory and practice of determining the mechanical and trybological properties of a wide range of materials and coatings by local loading of indenter at the macro-, micro- and nano-scales" of the National Academy of Sciences of Ukraine.

Author Contributions: Boris A. Galanov—development of the improved inclusion core model of the indentation process, wrote Theoretical background, Scheme and equations of the improved model; Yuly V. Milman—relation between the Tabor parameter $C = HM/Y_S$ and plasticity characteristic δ_H, wrote Results and Discussion, Conclusions; Svetlana I. Chugunova and Irina V. Goncharova—experimental part of the article, prepared figures and tables; Igor V. Voskoboinik—mathematical calculations.

Conflicts of Interest: The authors declare no conflict of interest.

References

1. Walley, S.M. Historical origins of indentation hardness testing. *Mater. Sci. Technol.* **2012**, *28*, 1028–1044.
2. Walley, S.M. Addendum and correction to 'Historical origins of indentation hardness testing'. *Mater. Sci. Technol.* **2013**, *29*, 1148.
3. Johnson, K.L. The correlation of indentation experiments. *J. Mech. Phys. Solids* **1970**, *18*, 115–126.
4. Johnson, K.L. *Contact Mechanics*; Cambridge University Press: Cambridge, UK, 1985.
5. Tanaka, K. Elastic/plastic indentation hardness and indentation fracture toughness: The inclusion core model. *J. Mater. Sci.* **1987**, *22*, 1501–1508.
6. Mata, M.; Anglada, M.; Alcala, J. A hardness equation for sharp indentation of elastic-power-low strain-hardening materials. *Philos. Mag. A* **2002**, *82*, 1831–1839.
7. Kogut, L.; Etsion, I. Elastic-plastic contact analysis of a sphere and a rigid flat. *J. Appl. Mech.* **2002**, *69*, 657–662.
8. Cheng, Y.-T.; Cheng, C.-M. Analysis of indentation loading curves obtained using conical indenters. *Philos. Mag. Lett.* **1998**, *77*, 39–47.
9. Cheng, Y.-T.; Cheng, C.-M. What is indentation hardness? *Surf. Coat. Technol.* **2000**, *133–134*, 417–424.
10. Galanov, B.; Milman, Yu.; Ivakhnenko, S.; Suprun, E.; Chugunova, S.; Golubenko, A.; Tkach, V.; Litvin, P.; Voskoboinik, I. Improved inclusion core model and its application for measuring the hardness of diamond. *J. Superhard Mater*. **2016**, *38*, 289–305.
11. Tabor, D. *The Hardness of Metals*; Clarendon Press: Oxford, UK, 1951.
12. Chaudhri, M.M. Strain hardening around spherical indentations. *Phys. Status Solidi A* **2000**, *182*, 641–652.
13. Brown, L.M. Indentation size effect and the Hall-Petch 'law'. *Mater. Sci. Forum* **2010**, *662*, 13–26.
14. Milman, Y.; Chugunova, S.; Goncharova, I. Plasticity at absolute zero as a fundamental characteristic of dislocation properties. *Int. J. Mater. Sci. Appl.* **2014**, *3*, 353–362.
15. Stelmashenko, N.A.; Walls, M.G.; Brown, L.M.; Milman, Y.V. Microindentation of W and Mo oriented single crystals: STM study. *Acta Metall. Mater.* **1993**, *41*, 2855–2865.
16. Nix, W.P.; Gao, H. Indentation size effects in crystalline materials: A law for strain gradient plasticity. *J. Mech. Phys. Solids* **1998**, *46*, 411–425.
17. McLaughlin, K.K.; Clegg, W.J. Deformation underneath low-load indentations in copper. *J. Phys. D Appl. Phys.* **2008**, *41*, 074007.
18. Milman, Y.V.; Galanov, B.A.; Chugunova, S.I. Plasticity characteristic obtained through hardness measurement. *Acta Metall. Mater.* **1993**, *41*, 2523–2532.
19. Gridneva, I.V.; Milman, Y.V.; Trefilov, V.I.; Chugunova, S.I. Analysis of dislocation mobility under concentrated loads at indentations of single crystals. *Phys. Status Solidi A* **1979**, *54*, 195–206.
20. Trefilov, V.I.; Milman, Y.V.; Grigoriev, O.N. Deformation and rupture of crystals with covalent interatomic bonds. *Prog. Cryst. Growth. Charact. Mater.* **1988**, *16*, 225–277.

21. Galanov, B.A.; Milman, Y.V.; Chugunova, S.I.; Goncharova, I.V. Investigation of mechanical properties of high-hardness materials by indentation. *J. Superhard Mater.* **1999**, *3*, 23.
22. Milman, Y.V.; Chugunova, S.I.; Goncharova, I.V. Plasticity characteristic obtained by indentation technique for crystalline and noncrystalline materials in the wide temperature range. *High Temp. Mater. Process.* **2006**, *25*, 39–46.
23. Milman, Y.V.; Miracle, D.B.; Chugunova, S.I.; Voskoboinik, I.V.; Korzhova, N.P.; Legkaya, T.N.; Podrezov, Y.N. Mechanical behaviour of Al_3Ti intermetallic and $L1_2$ phases on its basis. *Intermetallics* **2001**, *9*, 839–845.
24. Milman, Y.V. The effect of structural state and temperature on mechanical properties and deformation mechanisms of WC-Co hard alloy. *J. Superhard Mater.* **2014**, *36*, 65–81.
25. Milman, Y.V.; Luyckx, S.; Goncharuck, A.V.; Northrop, J.T. Results from bending tests on submicron and micron WC-Co grades at elevated temperatures. *Int. J. Refract. Met. Hard Mater.* **2002**, *20*, 71–79.
26. Gridneva, I.V.; Milman, Y.V.; Trefilov, V.I. Phase transition in diamond structure crystals at hardness measurement. *Phys. Status Solidi A* **1972**, *14*, 177–182.
27. Kovalchenko, A.M.; Milman, Y.V. On the cracks self-healing mechanism at ductile mode cutting of silicon. *Tribol. Int.* **2014**, *80*, 166–171.
28. Orlov, A.N.; Regel, V.R. Plasticity. In *Physical Encyclopedic Dictionary*; Soviet Encyclopaedia: Moscow, Russia, 1965; p. 39. (In Russian)
29. Plasticity (Physics), Wikipedia. Available online: https://en.wikipedia.org/wiki/Plasticity_%28physics%29 (accessed on 15 March 2017).
30. Milman, Y.V.; Chugunova, S.I.; Goncharova, I.V. Plasticity determined by indentation and theoretical plasticity of materials. *Bull. Russ. Acad. Sci. Phys.* **2009**, *73*, 1215–1221.
31. Bozzini, B.; Boniardi, M.; Fanigliulo, A.; Bogani, F. Tribological properties of electroless Ni-P/diamond composite films. *Mater. Res. Bull*. **2001**, *36*, 1889–1902.
32. Boldt, P.H.; Weatherly, G.C.; Embury, J.D. A transmission electron microscope study of hardness indentations in $MoSi_2$. *J. Mater. Res.* **2000**, *15*, 1025–1031.
33. Qiang, J.B.; Zhang, W.; Xie, G.; Kimura, H.; Dong, C.; Inoue, A. An in situ bulk $Zr_{58}Al_9Ni_9Cu_{14}Nb_{10}$ quasicrystal-glass composite with superior room temperature mechanical properties. *Intermetallics* **2007**, *15*, 1197–1201.
34. Lanin, A.G.; Lotsko, D.V.; Milman, Y.V.; Sibirtsev, S.A.; Fedorova, V.N.; Chugunova, S.I. The effect of temperature on the mobility of dislocations at the penetration of the indenter into a single crystal of molybdenum (001). *Phys. Met.* **1989**, *11*, 50–55. (In Russian)